Traveling Lamb wave in elastic metamaterial layer

Haisheng Shu [iD], Lihuan Xu, Xiaona Shi, Lei Zhao, and Jie Zhu

View Online   Export Citation   CrossMark

ARTICLES YOU MAY BE INTERESTED IN

Traveling Lamb wave in elastic metamaterial layer

Haisheng Shu,[1,2,a)] Lihuan Xu,[2] Xiaona Shi,[2] Lei Zhao,[2] and Jie Zhu[1,a)]

[1]*Department of Mechanical Engineering, The Hong Kong Polytechnic University, Hung Hom, Kowloon, Hong Kong SAR, China*
[2]*Mechanical & Electrical Engineering College, Harbin Engineering University, 150001 Harbin, China*

The propagation of traveling Lamb wave in single layer of elastic metamaterial is investigated in this paper. We first categorized the traveling Lamb wave modes inside an elastic metamaterial layer according to different combinations (positive or negative) of effective medium parameters. Then the impacts of the frequency dependence of effective parameters on dispersion characteristics of traveling Lamb wave were studied. Distinct differences could be observed when comparing the traveling Lamb wave along an elastic metamaterial layer with one inside the traditional elastic layer. We further examined in detail the traveling Lamb wave mode supported in elastic metamaterial layer, when the effective P and S wave velocities were simultaneously imaginary. It was found that the effective modulus ratio is the key factor for the existence of special traveling wave mode, and the main results were verified by FEM simulations from two levels: the level of effective medium and the level of microstructure unit cell. *Published by AIP Publishing.*
[http://dx.doi.org/10.1063/1.4965858]

I. INTRODUCTION

Phononic crystals are artificial periodic composite materials consisting of periodically distributed substructures or materials with high impedance contrast, which can give rise to many new wave phenomena such as band gap, defect mode, and negative refraction. These properties are mainly derived from the Bragg scattering effect of the elastic (or acoustic) wave at the periodic interfaces between internal components, and therefore, the working wavelength has to be on the same order as the lattice constant.[1] During the past decades, people have conducted extensive research on phononic crystals, such as the mechanisms of wave band gap and negative refraction,[2–4] tunable phononic crystals,[5–7] surface phononic crystals,[8,9] and phoxonic crystals.[10,11] In addition, the theory and experiment in recent years have demonstrated that phononic crystals can also be engineered to control thermal conductivity which is mainly influenced by phonon propagation (THz).[12–15] More information about phononic crystals can refer to Refs. 1 and 16.

Based on a kind of built-in localized resonances, Liu *et al.*[17] gives another concept of phononic crystals whose lattice constant can be two orders of magnitude smaller than the wavelength corresponding to its band gap. This kind of composite is now known as the local resonance type phononic crystals generally, or elastic metamaterials (EMs), if the host matrix of the building block (sub-wavelength unit cell) is a solid material.[18] Different from phononic crystals (Bragg type) where the periodicity is the decisive factor, the wave properties of EMs are mainly attributed to individual properties of the sub-wavelength unit cell with different resonant behaviors. Based on the concept of EMs, the elastic wave band gaps[19,20] have been

studied and the elastic wave cloaking[21,22] and negative refraction[23–25] have also been realized recently. At present, this field is still very active and more information about metamaterials can refer to Refs. 1 and 26.

As for EMs, the effective medium parameters can be taken to describe the dispersion properties of elastic waves in the long wavelength limit. Generally, the effective parameters of EMs are frequency-dependent, which leads to the dependency of the P wave and S wave velocities on frequency. In certain frequency regions, those effective parameters can become negative, owing to the vibrational eigenmodes of internal microstructure units. Such negative effective parameters may cause the waves inside having imaginary velocities (i.e., evanescent waves) to prohibit the propagation. A variety of microstructure units have been proposed to construct EMs.[27–31] Their frequency-dependent effective parameters were obtained by using effective medium theory. EMs with negative effective density, negative effective bulk modulus, negative effective shear modulus, or their different combinations (i.e., the single-, double-, or triple-negativities) have been realized.[18,19,32] In addition, preliminary studies on wave reflection and transmission occurring at the interface of two different EMs were carried out,[33] through which unique phenomena such as negative refraction and wave mode conversion were revealed. With those effective parameters not presented with natural materials, new EM designs were also proposed for the isolation of some important elastic waves, especially the seismic waves.[34–37]

Among all general cases of elastic wave propagation inside solid medium, how the wave travels in waveguides, such as elastic waveguide layer, is of great interest to both the fundamental scientific research and engineering applications. Although elastic wave motion in solid layered materials has been extensively studied, its research content is constantly enriched. When an elastic layer is constructed by

a)Authors to whom correspondence should be addressed. Electronic adresses: shujs@hrbeu.edu.cn and jie.zhu@polyu.edu.hk

using certain sub-wavelength unit cell with required local resonant properties as basic element, we can obtain an EM layer that may exhibit certain wave properties different from those of conventional elastic layer made of natural medium, due to the frequency dependence and negative characteristics of the effective medium parameters of the EM. Actually, some layers or plates composed of EMs have been investigated in recent years; some elastic wave phenomena like anisotropic mass density,[19] cloaking,[21,22] focusing,[24] band gap,[38,39] and energy localization[40] in such waveguides were observed within certain frequency ranges. Additionally, microstructural designs of plate-type EM and their potential applications were also reviewed.[41] However, the researches on wave propagation in EM layers are still relatively few and some problems need further investigations, e.g., the effects of the frequency-dependent and (or) negative effective medium parameters on the dispersion properties of Lamb wave, and the possibility of completely isolating the Lamb wave by means of EMs. In this paper, we will focus on the propagation of traveling Lamb wave in EM layers. Our findings suggest that, on one hand, the classical dispersion of traveling Lamb wave in elastic layer may have significant changes due to the frequency dependence of effective parameters induced by EM. On the other hand, the traveling Lamb wave in EM layer cannot be completely suppressed no matter which combination of negative parameters (single-, double-, or triple-negativities) is taken in EM design, unless certain requirement of effective modulus ratio is met. We believe that the results obtained here can definitely provide instructive information for future design of EMs, especially in the field of EM-based elastic wave isolation and object protection.

The paper is organized as follows. The model and basic wave equations together with the dispersion relations are given in Section II, and the traveling Lamb wave modes are categorized according to the combinations of positive or negative effective medium parameters. The only possible traveling Lamb wave mode is recognized when the effective P and S wave velocities are simultaneously imaginary. In Section III, we briefly demonstrate the effect of EM with typical frequency-dependent effective density on traveling Lamb wave dispersion characteristics. In Section IV, the unique traveling Lamb wave mode recognized in Section II is further discussed in detail. The supporting condition is mathematically proved. The theoretical results given in this part are also verified by FEM simulations from two levels: the level of effective medium and the level of microstructure unit cell. Finally, a concluding summary and potential future works are given in Section V.

II. MODE CLASSIFICATION OF THE TRAVELING LAMB WAVE

As schematically shown in Fig. 1, the upper and lower boundaries of the elastic layer are stress-free. The thickness is $2h$. The effective density, P wave modulus, and S wave modulus of the EM are denoted as $\rho_{eff}, E_{eff}, \mu_{eff}$, respectively. For homogeneous isotropic natural medium, E, μ, and ρ are positive constants and independent on wave frequency. However, when it comes to EMs, their artificially designed sub-
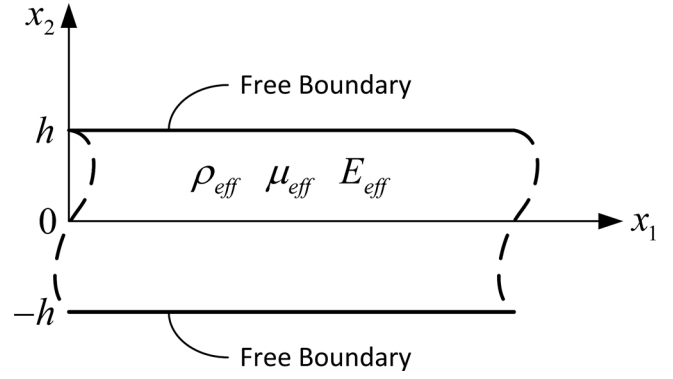
FIG. 1. Model of the EM Layer.

wavelength structures allow for spectral variation of effective parameters. Different negativities such as single-negativity, double-negativity, and triple-negativity within certain frequency bands are also achievable by subtle design of unit cells.

For the Lamb wave propagating in the layer, the displacement potentials can be written as (the detailed derivation is given in Appendix A)

$$\varphi = [A_1 \sin(px_2) + A_2 \cos(px_2)]e^{j(kx_1 - \omega t)}$$
$$\psi = [B_1 \sin(qx_2) + B_2 \cos(qx_2)]e^{j(kx_1 - \omega t)}, \quad (1)$$

where $p = \sqrt{\frac{\omega^2}{c_L^2} - k^2}, q = \sqrt{\frac{\omega^2}{c_T^2} - k^2}, \ c_L^2 = \frac{E}{\rho}, \ c_T^2 = \frac{\mu}{\rho}$ (For brevity, the subscripts of the effective parameter symbols are omitted here and hereafter), k is the wave number, p and q denote the P and S wave numbers, respectively, in the thickness direction (i.e., the x_2 direction) of the layer. Clearly, the real number of p (q) represents the shape of standing wave, while the imaginary number represents the form of evanescent wave in the thickness direction.

The solution in Equation (1) contains symmetric and antisymmetric wave components. According to the stress conditions of free boundaries ($x_2 = \pm h$), the famous Rayleigh-Lamb frequency equation can be subsequently written as

For symmetric mode

$$\frac{\tan(qh)}{\tan(ph)} = -\frac{4k^2pq}{(q^2 - k^2)^2}. \quad (2)$$

For antisymmetric mode

$$\frac{\tan(qh)}{\tan(ph)} = -\frac{(q^2 - k^2)^2}{4k^2pq}, \quad (3)$$

where the wave number k can take real, imaginary, or complex values.

Generally, for a given frequency, Equations (2) and (3) have limited number of real and purely imaginary solutions. Instead, the satisfying complex wave numbers are infinite in number. What we are interested here is the real wave number solutions, that is, the traveling wave modes which can propagate along the layer direction (the x_1 direction as shown in Fig. 1). In fact, these modes are more important in practical problems since they are directly related to the harmful elastic

TABLE I. Possible traveling wave solutions when the effective density of the EM is positive. **Re**—real number **Im**—imaginary number.

Effective density	Effective modulus	Effective wave velocity	Range of wave number	Properties of p and q
$\rho > 0$	$E > 0 \,\&\, \mu > 0$	$c_L^2 > 0 \,\&\, c_T^2 > 0$	$k < \omega/c_L \,\&\, k < \omega/c_T$	p: **Re** q: **Re**
			$k > \omega/c_L \,\&\, k > \omega/c_T$	p: **Im** q:**Im**
			$\omega/c_T < k < \omega/c_L$	p: **Re** q:**Im**
			$\omega/c_L < k < \omega/c_T$	p: **Im** q:**Re**
	$E > 0 \,\&\, \mu < 0$	$c_L^2 > 0 \,\&\, c_T^2 < 0$	$k > \omega/c_L$	p: **Im** q:**Im**
			$k < \omega/c_L$	p: **Re** q:**Im**
	$E < 0 \,\&\, \mu > 0$	$c_L^2 < 0 \,\&\, c_T^2 > 0$	$k > \omega/c_T$	p: **Im** q:**Im**
			$k < \omega/c_T$	p: **Im** q:**Re**
	$E < 0 \,\&\, \mu < 0$	$c_L^2 < 0 \,\&\, c_T^2 < 0$	...	p: **Im** q:**Im**

waves. Apparently, if k takes a positive real number, the wave numbers p (q) of P wave (S wave) in the thickness direction should be real or purely imaginary, and cannot be complex.

We have, therefore, summarized the possible traveling wave modes inside the EM layer according to the different combinations of positive or negative effective parameters. The results are shown in Tables I and II with the square of two effective wave velocities, and the wave numbers p and q. It is very clear that, on one hand, when all three effective parameters of the EM layer (ρ, E, and μ) are simultaneously positive or negative (namely, triple-positive or triple-negative), the constitution of the traveling wave solution in EM layer is similar to that in traditional elastic layer. The wave numbers in the thickness direction, i.e., p and q, have four different positive-negative combinations. Here, the determining factors for dispersion relations are the values of c_L^2 and c_T^2. Since they are positive in both triple-negative and triple-positive cases, the constitution of the traveling wave solution remains unchanged. On the other hand, if the number of negative effective parameters is less than three (namely, single-negative or double-negative), one or both of c_L^2 and c_T^2 would be negative, leading to the imaginary corresponding wave velocity (velocities) and the conversion of some of the traveling wave modes into evanescent modes. Therefore, the number of the traveling wave solutions reduces. As listed in Tables I and II, only two possible traveling wave modes remain when either c_L^2 or c_T^2 is negative. When c_L^2 and c_T^2 are both negative, we can anticipate one single traveling wave mode.

It is worth noting that, our study shows the traveling Lamb waves always exist in the EM layer and cannot be eliminated completely, no matter which combination of the effective parameters, i.e., the single-, double- or triple-

negatives, is taken. This is obviously different from the case of unbounded space, where all the elastic waves can be suppressed completely only by using EM with double-imaginary wave velocities (since all traveling wave modes are entirely converted into evanescent ones). This difference is due to the boundary effects. For the case of the EM layer with finite thickness, the two free boundaries will make the P wave and SV wave couple with each other. Moreover, they can also trigger surface traveling waves of which the P and (or) SV wave potentials take the shape of evanescent mode in the thickness direction of the EM layer. These surface traveling wave modes exist not only in the layers of natural mediums (triple-positive case), but also in the EM layers regardless of the combination of effective parameters.

As can be observed from Tables I and II, a special mode exists in all cases, i.e., the one of which both p and q are imaginary. More importantly, it may be excited as the only mode in two particular cases: $\rho < 0, E > 0, \mu > 0$ and $\rho > 0, E < 0, \mu < 0$, which correspond to the case with double-imaginary wave velocities. Apparently, this specific traveling wave mode deserves special attention, especially from the angle of elastic wave isolation, since it seems rather hard to be suppressed even though the EM with double-imaginary wave velocities is used.

III. DISPERSION CHARACTERISTICS WHEN EFFECTIVE PARAMETERS ARE FREQUENCY-DEPENDENT

All the three effective parameters of EM can be designed to be frequency-dependent, which have additional impacts on the dispersion relation of the Lamb wave in EM

TABLE II. Possible traveling wave solutions when the effective density of the EM is negative.

Effective density	Effective modulus	Effective wave velocity	Range of wave number	Properties of p and q
$\rho < 0$	$E > 0 \,\&\, \mu > 0$	$c_L^2 < 0 \,\&\, c_T^2 < 0$	–	p: **Im** q:**Im**
	$E > 0 \,\&\, \mu < 0$	$c_L^2 < 0 \,\&\, c_T^2 > 0$	$k > \omega/c_T$	p: **Im** q:**Im**
			$k < \omega/c_T$	p: **Im** q:**Re**
	$E < 0 \,\&\, \mu > 0$	$c_L^2 > 0 \,\&\, c_T^2 < 0$	$k > \omega/c_L$	p: **Im** q:**Im**
			$k < \omega/c_L$	p: **Re** q:**Im**
	$E < 0 \,\&\, \mu < 0$	$c_L^2 > 0 \,\&\, c_T^2 > 0$	$k < \omega/c_L \,\&\, k < \omega/c_T$	p: **Re** q: **Re**
			$k > \omega/c_L \,\&\, k > \omega/c_T$	p: **Im** q:**Im**
			$\omega/c_T < k < \omega/c_L$	p: **Re** q:**Im**
			$\omega/c_L < k < \omega/c_T$	p: **Im** q:**Re**

layer. The effects are exhibited directly through the effective P wave and S wave velocities. Here, we pick the effective density to be frequency-dependent to demonstrate the changes of dispersion curves. The effective P and S wave moduli remain positive constants. The effective density used here is borrowed from Ref. 30 (see Eq. (14) therein), and the Frequency Response Function (FRF) curve is shown in Fig. 2, where ω_0 is the characteristic frequency of the built-in unit of the EM (see the inset), ρ_{eff} and ρ_{st} represent the effective and static densities, respectively.

The dispersion equations (2) and (3) are solved numerically for a set of parameters: $h = 0.5\,\text{m}$, $E_{eff} = 10.84 \times 10^{10}\,\text{Pa}$, $\mu_{eff} = 2.87 \times 10^{10}\,\text{Pa}$, $\rho_{st} = 2700\,\text{kg/m}^3$. The dispersion curves are depicted in Fig. 3, where the horizontal axes are the dimensionless frequency thickness product and the vertical axes represent the real wave numbers (Figs. 3(a) and 3(b)) and phase velocities (Figs. 3(c) and 3(d)), respectively. For comparison, the dispersion curves of traditional elastic medium layer with static density ρ_{st} were also calculated and depicted in the figures.

As shown in Fig. 3, dispersion changes produced by introducing the frequency-dependent density are distinct. On one hand, the symmetric and antisymmetric mode curves tend to be similar as those of the constant density cases in the vicinity of zero frequency, where the system can be regarded as in a quasi-static state and the impact of frequency dependence is not prominent. However, when the wave frequency increases, eventually getting close to ω_0, the characteristic frequency of the internal unit of EM, the dispersion curves of these modes differ significantly from the classical results. The wave numbers of the curves shown in Figs. 3(a) and 3(b) will tend to reach infinity with the frequency approaching ω_0; therefore, the phase velocities will get close to zero simultaneously which can be seen clearly in Figs. 3(c) and 3(d). Meanwhile, the group velocities of these modes also approach zero when the frequency tends to ω_0 which can be found from the slope of the curves in Figs. 3(a) and 3(b), meaning that the energy of these wave modes can hardly be transferred. For the classical natural medium layer case, when the wave frequency approaches infinity, the phase velocities of A0 and S0 modes tend to the Rayleigh wave velocity, while those of all non-zero modes tend to the
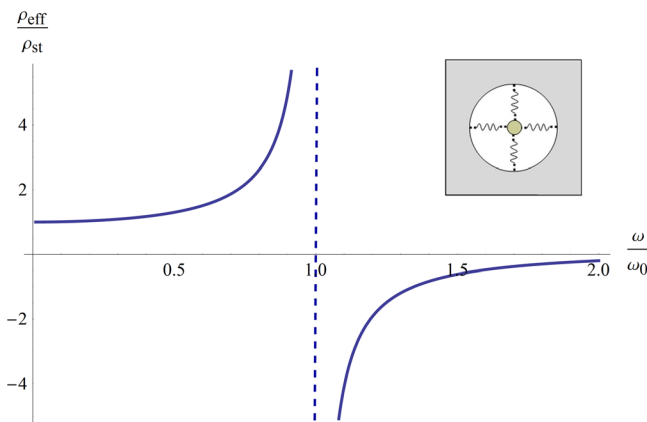
S wave velocity. However, if we check the EM layer, the two effective wave velocities, hence the effective Rayleigh wave velocity, decrease gradually. As shown in Fig. 2, they reach zero as the effective density increases and approaches infinity when the frequency increases close to ω_0. Thus, the phase velocities of both zero-order modes become zero, the effective Rayleigh wave velocity, while those of the non-zero modes will also tend to become zero, the effective S wave velocity.

In addition, in the classical natural medium layer case, the dispersion curves cover a wide frequency range. While for the EM layer, all the curves can be observed to be within the frequency region $0 < \omega < \omega_0$, and converge towards each other when the frequency approaches ω_0. This means the nonexistence of any traveling wave inside the EM layer when the frequency $\omega > \omega_0$. The two effective wave velocities are imaginary simultaneously since the effective density becomes negative, while both effective moduli are positive constants. In other words, a Lamb wave band gap is formed. Only the Lamb wave modes below this characteristic frequency ω_0 can go through, while those above will be blocked.

We mentioned in Sec. II that, a unique traveling mode with purely imaginary p and q can exist in the frequency region $\omega > \omega_0$ where both the two effective velocities are imaginary (see Table II). It is in contradiction with the conclusion we draw from the dispersion curves shown in Fig. 3. Thus, a natural question appears, i.e., indeed, is this unique traveling wave mode supported or not in the EM layer within the frequency region where the effective wave velocities are both imaginary?

IV. THE SPECIAL TRAVELING LAMB WAVE MODE WITH IMAGINARY *p* AND *q*

To answer the question raised above, we focus on the important case of which the effective P wave and S wave velocities are both imaginary. Actually, it contains two different combinations of effective parameters, namely, the case $\rho < 0, E > 0, \mu > 0$ and the case $\rho > 0, E < 0, \mu < 0$.

A. Further discussion on the dispersion relation

We start from the relationship between the phase velocity $c = \frac{\omega}{k}$ and the normalized frequency $\Omega = 2h\omega$ (frequency-thickness product). The dispersion relations (2) and (3) can be rewritten as

FIG. 2. FRF curve of the typical effective density.

$$\frac{\left(1 - e^{\frac{\Omega}{c}\sqrt{1 - \frac{c^2}{c_L^2}}}\right) \cdot \left(1 + e^{\frac{\Omega}{c}\sqrt{1 - \frac{c^2}{c_T^2}}}\right)}{\left(1 + e^{\frac{\Omega}{c}\sqrt{1 - \frac{c^2}{c_L^2}}}\right) \cdot \left(1 - e^{\frac{\Omega}{c}\sqrt{1 - \frac{c^2}{c_T^2}}}\right)}$$

$$= \frac{4\sqrt{\left(1 - \frac{c^2}{c_L^2}\right) \cdot \left(1 - \frac{c^2}{c_T^2}\right)}}{\left(\frac{c^2}{c_T^2} - 2\right)^2}, \tag{4}$$
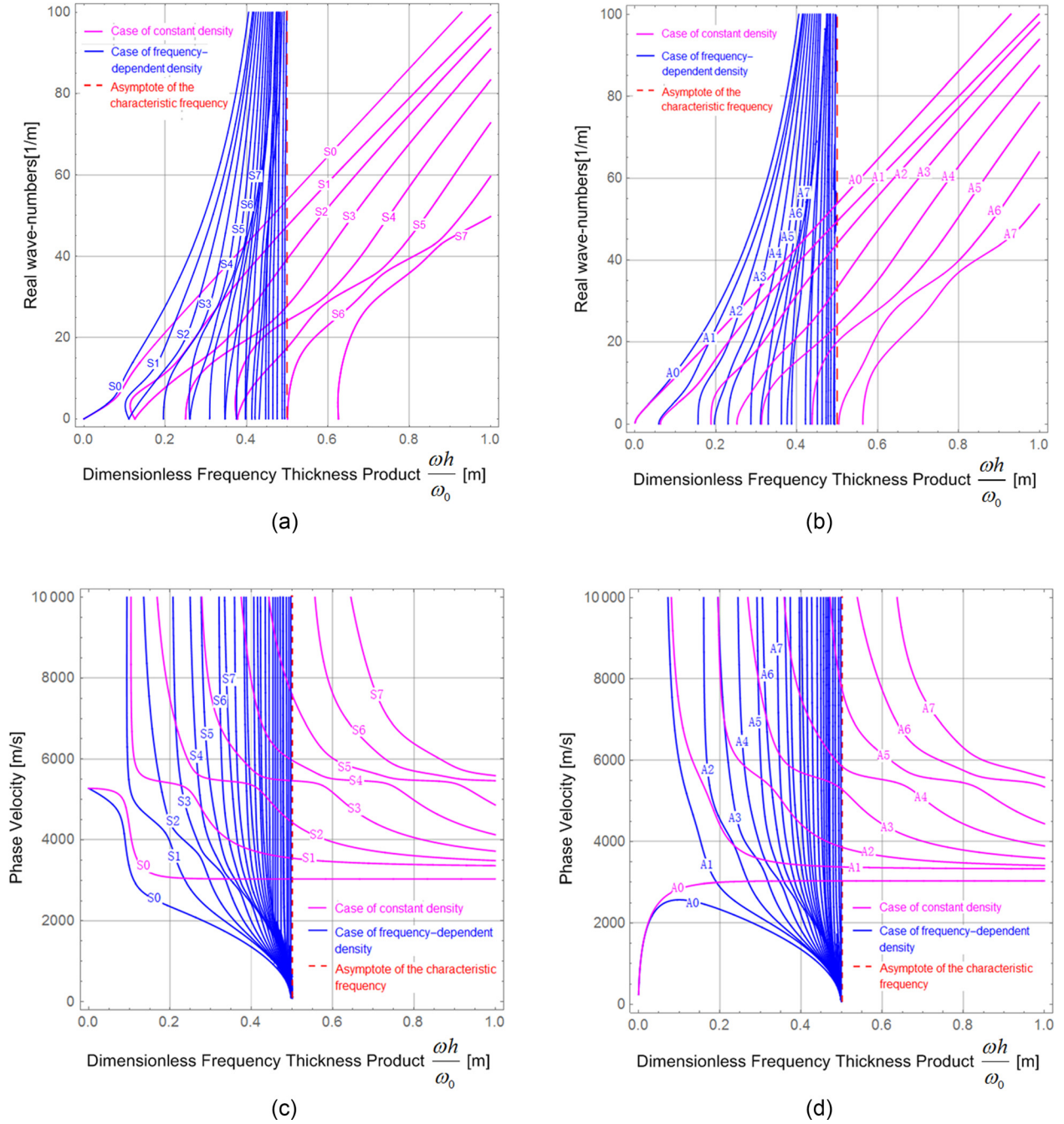
FIG. 3. Dispersion curves of the traveling Lamb wave modes propagating in traditional elastic layer and EM layer.

$$\frac{\left(1 - e^{\frac{\Omega}{c}\sqrt{1-\frac{c^2}{c_L^2}}}\right) \cdot \left(1 + e^{\frac{\Omega}{c}\sqrt{1-\frac{c^2}{c_T^2}}}\right)}{\left(1 + e^{\frac{\Omega}{c}\sqrt{1-\frac{c^2}{c_L^2}}}\right) \cdot \left(1 - e^{\frac{\Omega}{c}\sqrt{1-\frac{c^2}{c_T^2}}}\right)}$$

$$= \frac{\left(\frac{c^2}{c_T^2} - 2\right)^2}{4\sqrt{\left(1 - \frac{c^2}{c_L^2}\right) \cdot \left(1 - \frac{c^2}{c_T^2}\right)}}. \qquad (5)$$

To facilitate the discussion, the effective modulus ratio $\sigma = \frac{E}{\mu} = \frac{c_L^2}{c_T^2}$ is introduced here. It can also be expressed as the

effective wave velocity ratio $\sqrt{\sigma} = \frac{c_L}{c_T}$. For simplicity, we bring in four additional parameters, $b = \frac{\Omega}{c}$, $a = -\frac{c^2}{c_T^2}$, $m = \sqrt{1+a}$, $s = \sqrt{1+\frac{a}{\sigma}}$, where $b > 0, a > 0, m > 1, s > 1$ are required. Then, the Equations (4) and (5) can be reduced as follows:

For symmetric mode

$$\frac{(e^{bs} - 1) \cdot (e^{bm} + 1)}{(e^{bs} + 1) \cdot (e^{bm} - 1)} = \frac{4ms}{(m^2 + 1)^2}. \qquad (6)$$

For antisymmetric mode

$$\frac{(e^{bs} - 1) \cdot (e^{bm} + 1)}{(e^{bs} + 1) \cdot (e^{bm} - 1)} = \frac{(m^2 + 1)^2}{4ms}. \qquad (7)$$

When $\sigma \geq 1$, $1 < s \leq m$. The left-hand side (LHS) of Eq. (7) is less than or equal to 1, while the right-hand side (RHS) is always greater than 1. Therefore, the equation cannot be satisfied at all, meaning that no antisymmetric traveling wave modes occur under this circumstance.

As for Eq. (6), the RHS is indeed less than 1 which seems to indicate that Eq. (6) could have valid solution in the form of existing symmetric traveling wave. However, if we construct the following function:

$$f(s) = \frac{(e^{bs} - 1) \cdot (e^{bm} + 1)}{(e^{bs} + 1) \cdot (e^{bm} - 1)} \cdot \frac{(m^2 + 1)^2}{4ms} - 1.$$

Then, Eq. (6) is equivalent to $f = 0$. Now let us assume that $s = m$; it can be seen that $f(m) = \frac{(m^2 - 1)^2}{4m^2} > 0$. The first derivative of function f with respect to s is

$$\frac{df}{ds} = \frac{e^{bm} + 1}{e^{bm} - 1} \cdot \frac{(m^2 + 1)^2}{4m} \cdot \frac{d}{ds}\left\{\frac{1}{s} \cdot \frac{e^{bs} - 1}{e^{bs} + 1}\right\}$$
$$= \frac{e^{bm} + 1}{e^{bm} - 1} \cdot \frac{(m^2 + 1)^2}{4m} \cdot \frac{1}{s^2(e^{bs} + 1)^2}$$
$$\cdot [1 + e^{bs}(2bs - e^{bs})]. \quad (8)$$

When $bs > 0$, we have $1 + e^{bs}(2bs - e^{bs}) < 0$, and subsequently $\frac{df}{ds} < 0$. Therefore, $f(s) \geq f(m) > 0$ is obtained since $1 < s \leq m$, which means $f = 0$ is invalid and hence Eq. (6) cannot be satisfied. Obviously, it can be concluded that when the proposed effective modulus ratio parameter $\sigma \geq 1$, the special traveling wave mode with imaginary p and q cannot exist in the frequency region where the two effective wave velocities are imaginary. With the parameters we used to calculate the dispersion curves presented in Fig. 3, $\sigma = \frac{E}{\mu} = \frac{10.84}{2.87} = 3.8 > 1$, eventually leading to the no observation of such traveling wave mode.

Now there is another scenario of $0 < \sigma < 1$. With the aid of similar analysis process, it can be proved that the Eqs. (4) and (5) (or Eqs. (6) and (7)) have solutions. Nevertheless, the explicit expressions of their solutions cannot be obtained and only numerical ones may be presented. We have calculated them by giving the parameters a set of specific values ($\sigma = 0.35, 0.50, 0.66, 0.80, 0.95$, $c_T = 3200\,i\,(\text{m/s})$). The results are shown in Fig. 4 with the symmetric and antisymmetric modes represented by solid lines and dotted lines, respectively. For simplicity purpose, these parameters are assumed to be nondispersive and constants within the whole frequency band. It is clear that these curves are just the counterparts of the A0 and S0 modes in classical results. However, the components of wave modes contained are with imaginary p and q. Additionally, no traveling wave modes of non-zero order appears.

We would like to discuss the characteristics of the symmetric mode first. When the frequency-thickness product approaches zero, i.e., $\Omega \to 0$ ($\Omega = 2h\omega$), $\frac{c}{|c_T|} \to 2\sqrt{\frac{1}{\sigma} - 1}$ ($|\cdot|$ represents modulus operation) can be obtained by using L Hospitals rule. The phase velocity c of the traveling wave mode tends to reach a fixed value determined by σ and $|c_T|$, when the frequency reaches the lower limit. According to the
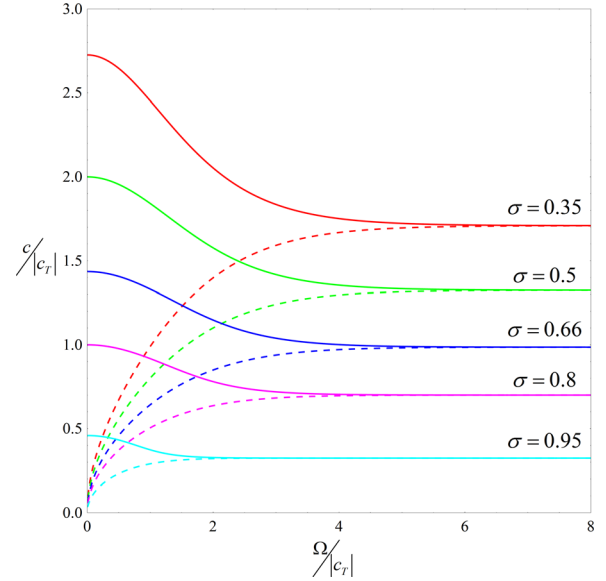
FIG. 4. Dispersion curves of the traveling wave mode with imaginary p and q: $\sigma < 1$.

set of values of σ given above, these fixed values of phase velocity c are obtained as follows: 2.73, 2.00, 1.44, 1.00, 0.46. They are also the vertical ordinates of the intersection points of the solid lines and the vertical axis in Fig. 4. As the frequency increases, the symmetric wave velocity decreases gradually and approaches a fixed value when $\Omega \to \infty$ (the details can be found in Appendix B), which is similar to the classical elastic wave case where the velocity eventually tends to reach the Rayleigh wave velocity.

Similar analysis process can be conducted for the antisymmetric mode. Considering $\Omega \to 0$ and $\Omega \to \infty$, we find $c \to 0$ when $\Omega \to 0$, and reach Eq. (A4) once again when $\Omega \to \infty$. Therefore, the phase velocities of the symmetric and antisymmetric modes tend towards the same fixed value, namely, the Rayleigh wave velocity ($\sqrt{a} \cdot |c_T|$), (see also Appendix B) of the EM layer.

It should be noted that, the constant σ and c_T are assumed in above analyses for simplicity. However, these parameters are always frequency-dependent for real EMs, and hence, no such EM layer can have the dispersion curves given in Fig. 4. In spite of this, these curves are still meaningful. In fact, for any practical EM layer possessing double imaginary wave velocities and satisfying $0 < \sigma < 1$ within certain frequency region, every point of its practical dispersion curve (i.e., the unique traveling wave mode with imaginary p and q) should be located on one of these curves (like those given in Fig. 4) according to its corresponding σ and c_T values.

B. Finite Element Simulation based on the model of effective medium

Finite element simulations were carried out by using the software COMSOL Multiphysics 5.0. A two-dimensional simulation model is used here with line load applied at the left boundary. The mesh model is shown in Fig. 5, where the EM layer is 8 m with a PML layer of 2 m in length, and
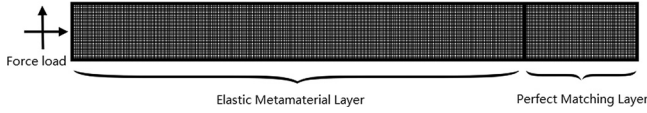
FIG. 5. Finite element mesh model.

the thickness is 1 m. In the case of symmetric loading, two loads in different directions are applied on the upper half section of the layer's left boundary, one direction is towards the right and the other is straight up, while the load directions on the lower half section are towards the right and straight down. On the other hand, for the antisymmetric loading case, the loading directions on the upper half section are towards the right and straight up, and the loading directions on the lower half section are towards the left and straight up. All the loads have the same amplitudes (10 kN/m) and phases.

In the following, two different cases, i.e., $0 < \sigma < 1$ and $\sigma > 1$, were considered, respectively. Since the simulation here is based on the model of effective medium, the simulation model is assumed to be homogeneous and isotropic.

(1) $0 < \sigma < 1$

Here we select $\sigma = 0.66$, $c_T = 3200\,i$ (m/s), and two frequency points (4 kHz and 0.8 kHz) for calculations. In order to facilitate the comparison with the following simulation results, the dispersion curves of EM layer with the same parameters are computed first according to Eqs. (6) and (7), and the results are depicted in Fig. 6. The wave velocities corresponding to the selected frequencies are also marked in Fig. 6. At 4 kHz, the velocities of the symmetric and antisymmetric modes are same value 3154 m/s and the wavelength is about 0.78 m. At 800 Hz, the velocity of the symmetrical mode (red solid line) is 3910 m/s, while that of the antisymmetric mode (blue dotted line) is 2483 m/s. The corresponding wavelengths are around 4.89 m and 3.10 m, respectively.
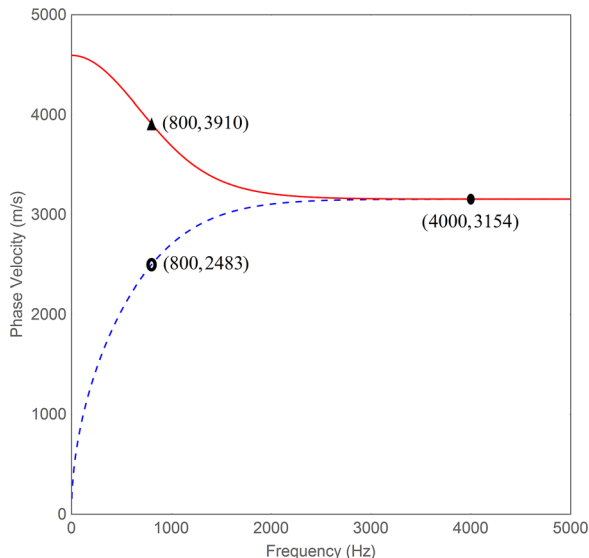
FIG. 6. Dispersion curves under the condition: $\sigma = 0.66$, $c_T = 3200\,i$ (m/s).

(a)   The simulation results at 4 kHz.
      Figure 7 shows the displacement field fluctuations at 4 kHz in the EM layer. It can be observed that the propagation of expected traveling wave in the EM layer is rather clear although the effective wave velocities are both imaginary. From the simulation results, the displacement field close to the center of EM layer is almost zero. The traveling waves are only visible in a form of surface wave near the free surfaces, indicating the imaginary values of p and q. Further examination of the displacement field shows that both the symmetric and antisymmetric modes of the traveling wave have the same wavelength (around 0.76 m) as marked in Figs. 7(c) and 7(f), in good agreement with the theoretical result (0.78 m).

(b)   The simulation results at 0.8 kHz.
      Fig. 8 shows the simulated displacement field in the EM layer at 0.8 kHz. It can be seen that significant traveling wave still exists at this low frequency. Those traveling wave modes with imaginary p and q still appear mainly in the vicinity close to the free surfaces. However, since the corresponding wavelengths are relatively large, the displacement fields inside the layer are much more remarkable than those at 4 kHz. Through measuring the distance between displacement peaks as marked in Fig. 8, it is found that the wavelengths of the symmetric and antisymmetric modes are around 4.87 m and 3.11 m, respectively, fairly consistent with theoretical results (4.89 m and 3.10 m, respectively).
      All the results at the two frequencies show that, when $0 < \sigma < 1$, EM layer can support significant traveling wave in surface wave form, even though both of the effective P and S wave velocities are imaginary simultaneously.

(2) $\sigma > 1$

In this part, we select $\sigma = 1.5$ and keep all other parameters in the previous case. The distributions of wave fields at the two frequencies, 4 kHz and 0.8 kHz are simulated and depicted in Figs. 9 and 10. Apparently, no traces of traveling wave can be observed in the EM layer in both cases, which further confirms the prediction from our theoretical analysis. Now if one would like to suppress or completely isolate the elastic waves propagating in a waveguide layer with the introduction of EM having double-imaginary effective wave velocities, a requirement that has to be met is $\sigma > 1$. So the EM layer will be able to eliminate all possible traveling waves so as to achieve the desired elastic wave isolation and target protection.

C. Finite Element Simulation based on the microstructure unit cell of EM

To verify the theoretical results with practical materials, an appropriate unit cell of EM is borrowed from Ref. 42, however, the triangular lattice is replaced by a square lattice here for convenience. It is composed of three-component
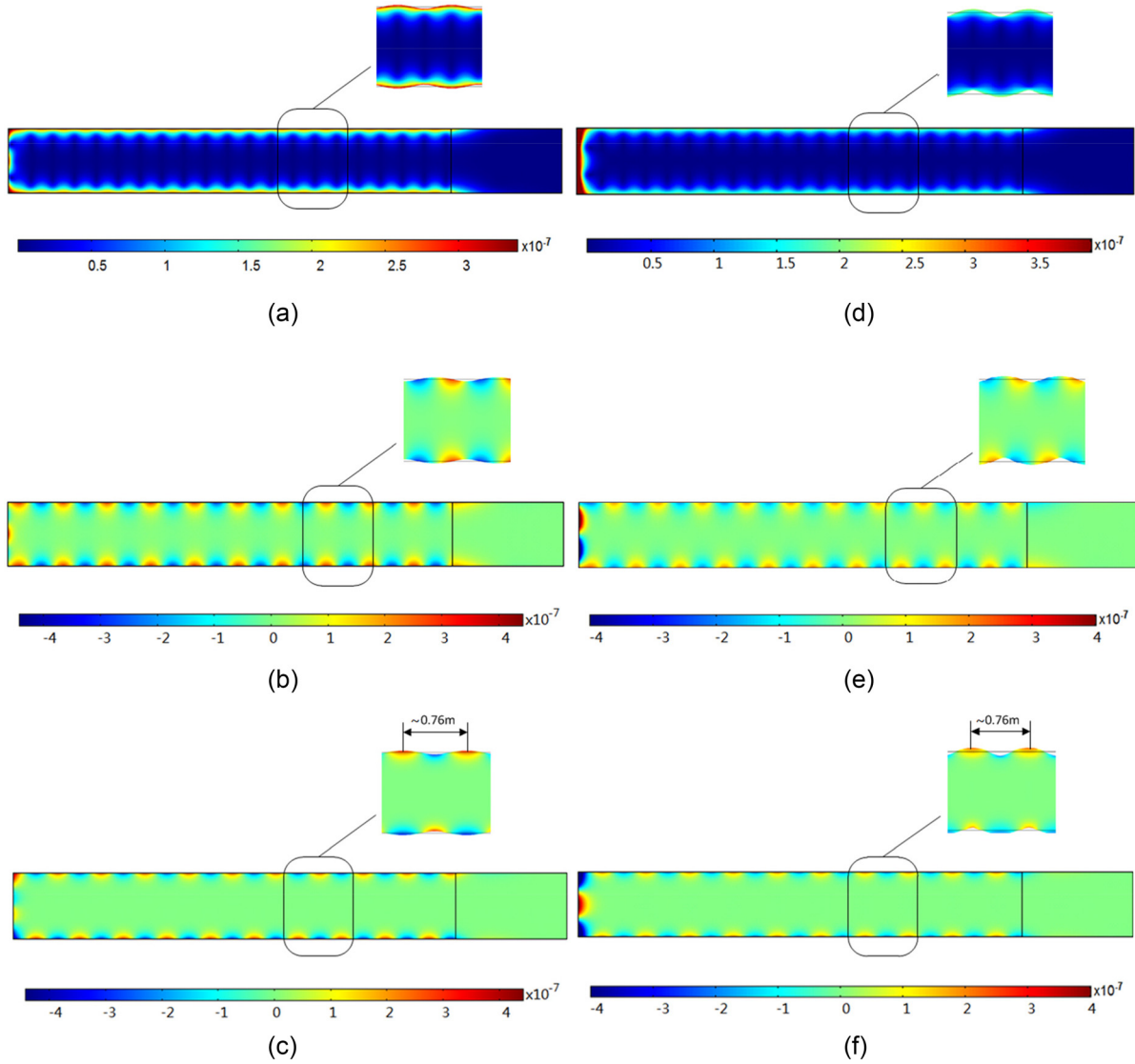
FIG. 7. Traveling wave mode with imaginary p and q in the EM layer possessing double imaginary effective wave velocities: $\sigma = 0.66$, 4 kHz.

continuum media by a Polyethylene coated lead cylinder embedded in Epoxy matrix. The structural parameters are given in Fig. 11 (left panel, unit: mm) and the material properties are as follows:

Polyethylene: density $920\,\mathrm{kg/m^3}$, bulk modulus 0.57×10^9 Pa, shear modulus 0.13×10^9 Pa;
Lead: density $11600\,\mathrm{kg/m^3}$, bulk modulus 52.6×10^9 Pa, shear modulus 14.9×10^9 Pa;
Epoxy: density $1110\,\mathrm{kg/m^3}$, bulk modulus 3.14×10^9 Pa, shear modulus 0.89×10^9 Pa.

The band structure along the ΓX direction for the square lattice is presented also in Fig. 11 (right panel). In addition, the effective parameters of the EM built with the unit cells are calculated by using the numerical method proposed also in Ref. 42, and the normalized effective mass density, bulk modulus, and shear modulus are depicted in Fig. 12, where the symbol a is lattice constant (10 mm) and $\tilde{c}$ is the S wave velocity of the matrix (epoxy).

The band structure shows that the first band gap is located within the normalized frequency region $0.190 \sim 0.201$ where ρ_{eff} is negative and E_{eff} ($E_{eff} = \kappa_{eff} + \mu_{eff}$, the effective longitudinal wave modulus) and μ_{eff} are both positive (actually, μ_{eff} remains positive and almost unchanged within the interested frequency range), i.e., both of the effective P wave and S wave velocities are imaginary. With the increase of wave frequency, κ_{eff} decreases gradually and tends to become $-\infty$ below frequency 0.218. Apparently, E_{eff} will become negative when beyond certain frequency point (0.201 here); therefore, a negative energy band curve occurs owing to ρ_{eff} and E_{eff} negative simultaneously which can be observed in Fig. 11 (right panel). In this frequency band ($0.201 \sim 0.218$), the effective S wave velocity is imaginary while the P wave velocity is real. Additionally, there exists second band gap in the frequency band $0.218 \sim 0.410$ where both the wave velocities become imaginary again (i.e., $\rho_{eff} < 0, E_{eff} > 0, \mu_{eff} > 0$) since κ_{eff} turns positive beyond 0.218.

Twelve cells are adopted along the thickness direction to construct the EM layer. The surface Lamb wave modes of the EM layer are calculated by super cell simulation with software COMSOL 5.0. The calculated dispersion curves of the surface Lamb wave modes are shown in Fig. 13 by the
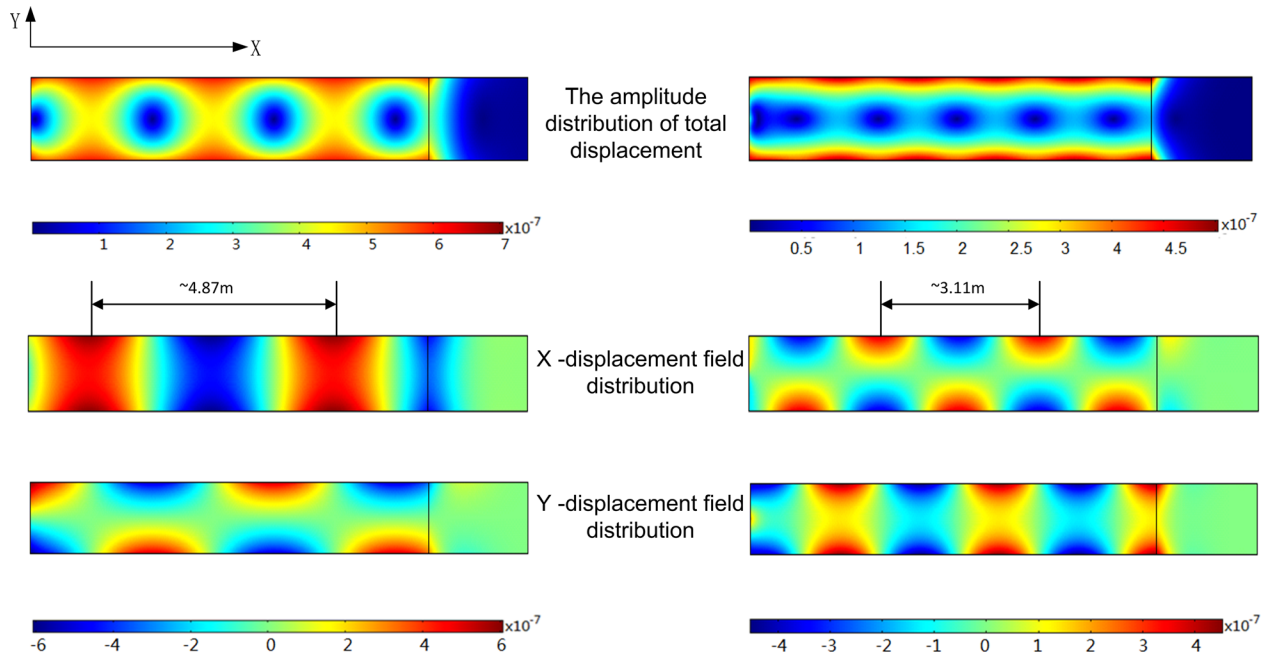
FIG. 8. Traveling wave mode with imaginary p and q in the EM layer possessing double imaginary effective wave velocities: $\sigma = 0.66, 0.8\,\text{kHz}$.
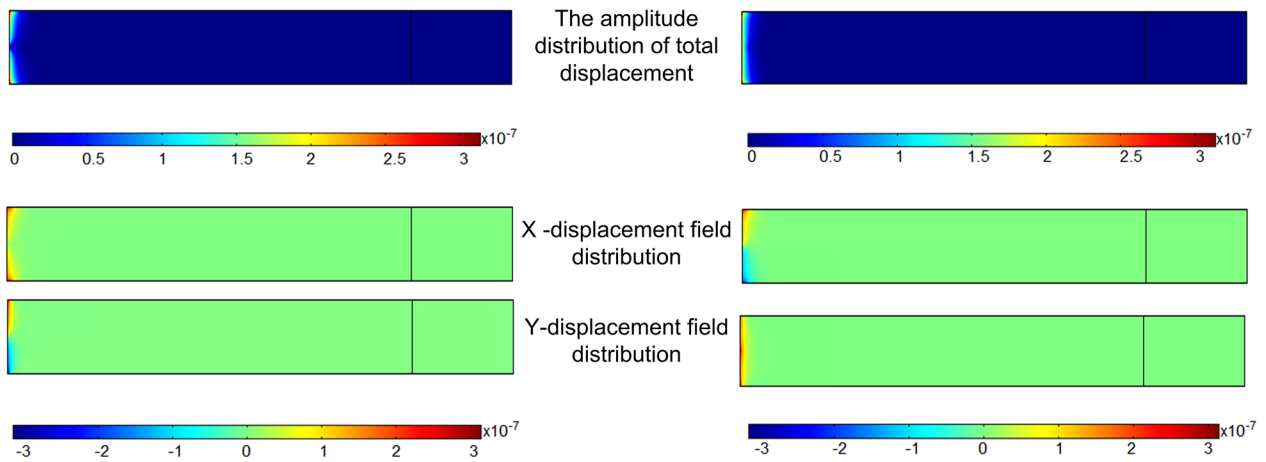
FIG. 9. No traveling wave occurring in the EM layer of which both effective wave velocities are imaginary: $\sigma = 1.5, 4\,\text{kHz}$.
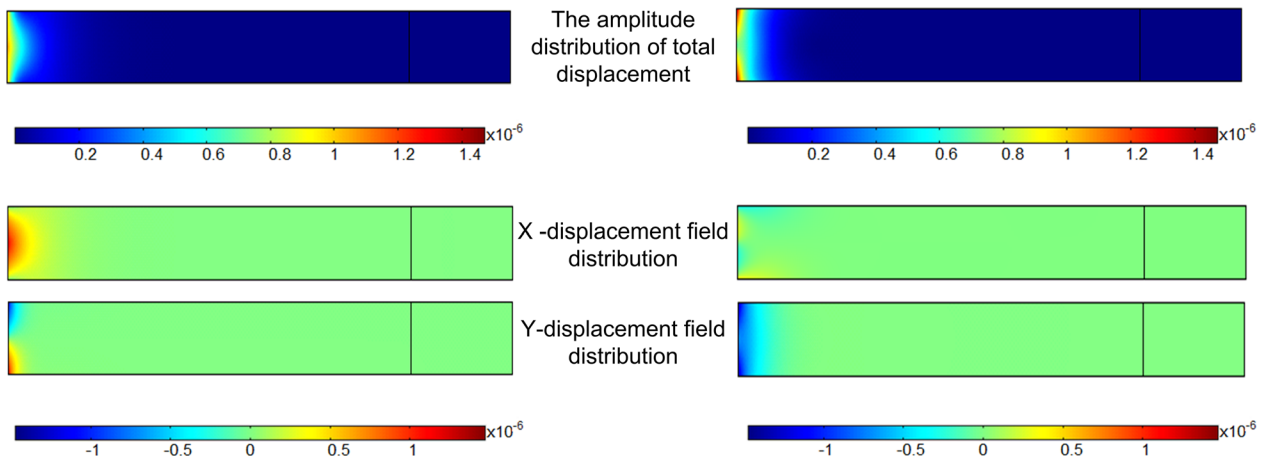
FIG. 10. No traveling wave occurring in the EM layer of which both effective wave velocities are imaginary: $\sigma = 1.5, 0.8\,\text{kHz}$.

(a)

(b)
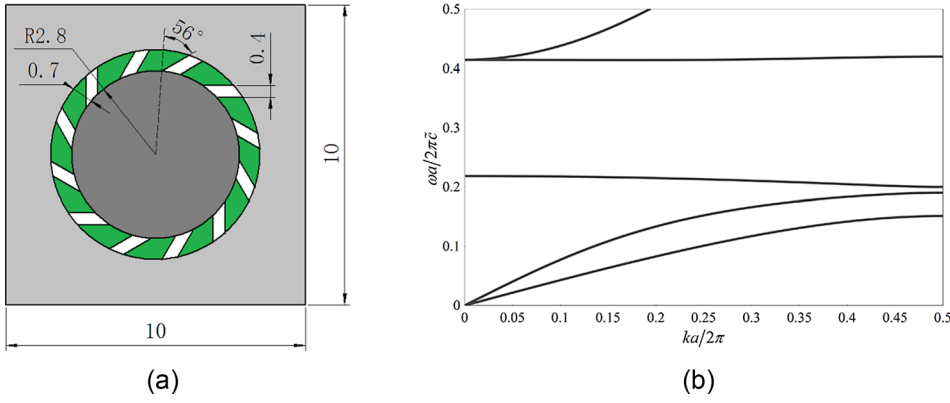
FIG. 11. Unit cell of the 2D EM and its band structure.
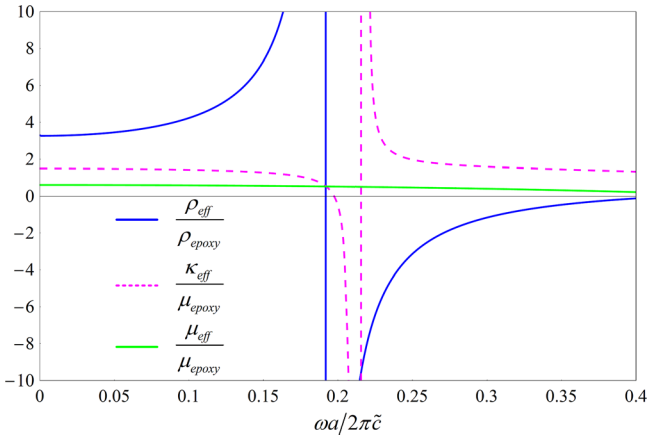
FIG. 12. Effective parameters of the EM.

star markers (antisymmetric mode) and plus sign markers (symmetric mode). For convenience, part of the band structure of the unit cell is also given in Fig. 13. Clearly, small parts of the dispersion curves of the surface Lamb wave mode fall within the first band gap of the band structure of the unit cell. They are very close to the lower edge of the negative energy band curve of the unit cell and just the predicted unique traveling Lamb wave modes with imaginary p and q, since both of the effective P and S wave velocities are imaginary. As a matter of fact, E_{eff} equals to 0 just at the lower edge of the negative energy band curve (normalized frequency 0.201), in another word, $\kappa_{eff} = -\mu_{eff}$. When the
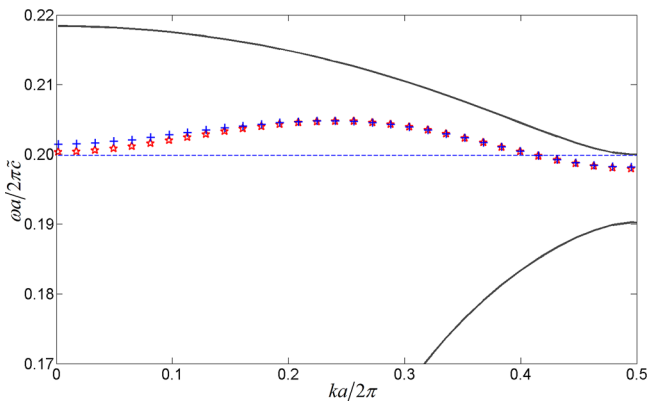
wave frequency decreases gradually from the point, E_{eff} will become positive and increase gradually since κ_{eff} increases at the same time (see Fig. 12). During the process, the condition $0 < \sigma < 1$ will be satisfied until κ_{eff} equals to 0 (corresponding frequency is around 0.197), and therefore the unique traveling Lamb wave modes will exist in the normalized frequency region $0.197 \sim 0.201$ which agrees with Fig. 13 well. Below frequency 0.197, κ_{eff} turns positive and hence E_{eff} is bigger than μ_{eff}, meaning that the occurring condition of the unique traveling Lamb wave mode is not reached any longer.

The displacement field distributions of the surface Lamb wave modes with normalized wave number $ka/2\pi = 0.49$ are given in Fig. 14. It can be observed that these modes are really confined near to the free surfaces of the EM layer, and the symmetric and anti-symmetric modes can also be identified.

V. SUMMARY AND CONCLUSION

The traveling Lamb wave modes in EM layer are discussed based on the effective medium parameters in this paper. According to different combinations of positive or negative effective parameters, the possible traveling wave modes in the layer are categorized. Then, the impacts of the frequency dependency of typical effective density on the dispersion characteristics are investigated. Finally, we focus on the existential condition of a unique traveling wave mode (i.e., the one with imaginary p and q) and discuss it in detail. Our research shows that

(1) The traveling elastic wave solutions change with different combinations of effective parameters, owing to the distinct effective P wave and S wave velocities. The EM layer supports different number of possible traveling wave modes according to the wave numbers in the

FIG. 13. Surface Lamb wave modes located in the band gap of bulk wave, calculated by a super cell simulation of 12 cells.

(a) Symmetric mode

(b) Antisymmetric mode
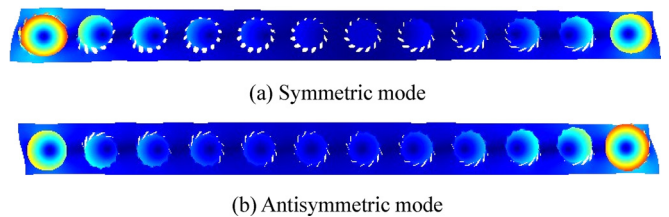
FIG. 14. Field distributions of the surface Lamb wave modes with $ka/2\pi = 0.49$.

thickness direction (p and q): four, if the effective P and S wave velocities are both real; two, if either of the effective wave velocities is imaginary while another remains real; and only one possible traveling wave mode with imaginary p and q when both of the effective wave velocities are imaginary.

(2) The frequency dependency of the effective parameters has significant impacts on the dispersion characteristics of the traveling Lamb wave in EM layer. Although we cannot discuss all the possible frequency dependencies one by one, the conclusion is confirmed by analyzing a typical and common effective density case. For example, the dispersion curves concentrate in the frequency region $0 < \omega < \omega_0$ and converge together when approaching the characteristic frequency ω_0 of the EM unit cell. Meanwhile, the phase velocities of all symmetric and antisymmetric branches tend to reach zero. Moreover, all the traveling wave modes vanish completely above ω_0 when $\sigma \geq 1$.

(3) For the EM layer with double-imaginary effective wave velocities, whether the only possible traveling wave mode (with imaginary p and q) appears or not depends on the value of the effective modulus ratio σ (or the effective wave velocity ratio $\sqrt{\sigma}$). When $\sigma \geq 1$, this unique mode is not supported and ideal wave isolation can be realized. However, such mode will come into being in the EM layer when $0 < \sigma < 1$. When it does exist, this traveling mode is mainly concentrated in the vicinity around the two free surfaces, hence, it is a kind of surface wave. Since it is not attenuated along the propagation direction without considering damping effects, this surface traveling wave needs to be monitored if we wish to achieve elastic wave isolation with the EM layer. On the other hand, it may contribute to the production of pure surface wave mode in waveguide structure, which is hard to achieve with natural elastic medium layers.

Various types of waveguides are commonly used in practical applications. Analyzing the waves inside those structures is rather important. We have conducted a theoretical and numerical study on the traveling Lamb wave in the EM waveguide layer based on the dispersion equations. The potential future direction to explore includes two major aspects: first, it is meaningful for overall understanding to investigate the traveling wave characteristics of other cases listed in Tables I and II; second, it is also important to consider some other practical waveguides such as multi-layer materials built with EMs and half space with EM coating.

ACKNOWLEDGMENTS

APPENDIX A: BASIC THEORETICAL DERIVATION FOR EQ. (1)

For Lamb wave propagating in the elastic metamaterial layer (shown in Fig. 1), the basic equations of the displacement potentials can be written as[43]

$$\frac{\partial^2 \varphi}{\partial x_1^2} + \frac{\partial^2 \varphi}{\partial x_2^2} = \frac{1}{c_L^2} \frac{\partial^2 \varphi}{\partial t^2}$$
$$\frac{\partial^2 \psi}{\partial x_1^2} + \frac{\partial^2 \psi}{\partial x_2^2} = \frac{1}{c_T^2} \frac{\partial^2 \psi}{\partial t^2}, \tag{A1}$$

where $c_L^2 = \frac{E}{\rho}, c_T^2 = \frac{\mu}{\rho}$ (For brevity, the subscripts of the effective parameter symbols are omitted).

The relationship between the displacements and the displacement potentials is

$$u_1 = \frac{\partial \varphi}{\partial x_1} + \frac{\partial \psi}{\partial x_2}$$
$$u_2 = \frac{\partial \varphi}{\partial x_2} - \frac{\partial \psi}{\partial x_1}. \tag{A2}$$

Substituting the formal solution $\phi = \Phi(x_2)e^{j(kx_1 - \omega t)}$, $\psi = \Psi(x_2)e^{j(kx_1 - \omega t)}$ in Eq. (A1), we obtain

$$\varphi = [A_1 \sin(px_2) + A_2 \cos(px_2)]e^{j(kx_1 - \omega t)}$$
$$\psi = [B_1 \sin(qx_2) + B_2 \cos(qx_2)]e^{j(kx_1 - \omega t)}, \tag{A3}$$

where $p = \sqrt{\frac{\omega^2}{c_L^2} - k^2}, q = \sqrt{\frac{\omega^2}{c_T^2} - k^2}$, k is the wave number, p and q denote the P and S wave numbers, respectively, in the thickness direction (i.e., the x_2 direction) of the layer.
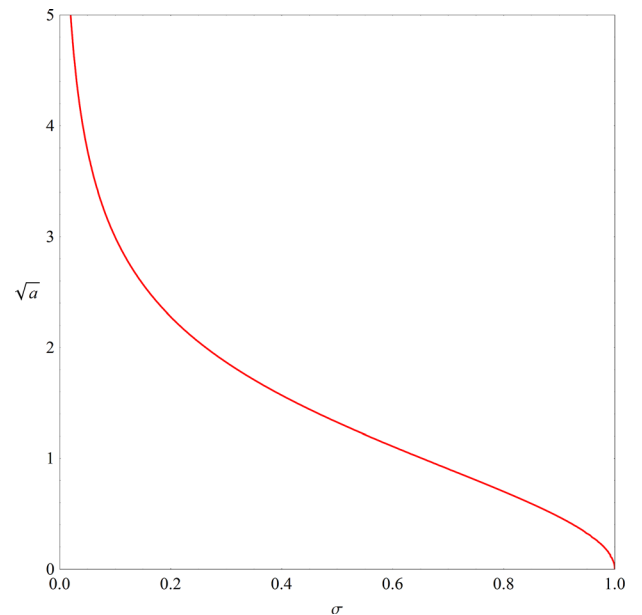
FIG. 15. Numerical solutions of Equation (A4).

APPENDIX B: DETAILS OF THE SYMMETRIC WAVE VELOCITY AS $\Omega \to \infty$

When $\Omega \to \infty$, the equation that relates the wave velocity ratio $(a = -\frac{c^2}{c_T^2})$ to the effective modulus ratio $(\sigma = \frac{E}{\mu} = \frac{c_L^2}{c_T^2})$ can be derived from Eq. (6)

$$(a + 2)^2 = 4\sqrt{(1 + a)\left(1 + \frac{a}{\sigma}\right)}. \qquad (A4)$$

Obviously, Equation (A4) has the same form as the phase velocity equation of Rayleigh wave. Despite this, it should be noted that the value of a is positive here and $0 < \sigma < 1$, while the value of a in the phase velocity equation of Rayleigh wave is negative $(a = -\frac{c^2}{c_T^2}, c^2 > 0)$ and $\sigma > 1$ $(\sigma = \frac{c_L^2}{c_T^2}, c_L > c_T)$. The numerical solution of Eq. (A4) has been shown in Fig. 15. Apparently, with σ $(0 < \sigma < 1)$ decreasing gradually, the value of $\sqrt{a}$ increases monotonically, leading to the phase velocity increase of the traveling wave mode $(c = \sqrt{a} \cdot |c_T|)$. This is consistent with the trend shown in Fig. 4.

[1] P. A. Deymier, *Acoustic Metamaterials and Phononic Crystals* (Springer-Verlag, Berlin, Heidelberg, 2013).
[2] Liang Feng, Xiao-Ping Liu, Ming-Hui Lu *et al.*, "Acoustic backward-wave negative refractions in the second band of a sonic crystal," Phys. Rev. Lett. **96**(1), 014301 (2006).
[3] L.-Y. Wu, L.-W. Chen, and R. C.-C. Wang, "Dispersion characteristics of negative refraction sonic crystals," Physica B: Condens. Matter **403**, 3599 (2008).
[4] S. Alagoz, B. B. Alagoz, and A. Sahin, "Negative refractions by triangular lattice sonic crystals in partial band gaps," Chin. Phys. B **24**(4), 046201 (2015).
[5] K. Bertoldi and M. C. Boyce, "Mechanically triggered transformations of phononic band gaps in periodic elastomeric structures," Phys. Rev. B **77**, 052105 (2008).
[6] Y.-Z. Wang, F.-M. Li, W.-H. Huang, X. Jiang, Y.-S. Wang, and K. Kishimoto, "Wave band gaps in two-dimensional piezoelectric/piezomagnetic phononic crystals," Int. J. Solids Struct. **45**, 4203 (2008).
[7] H. Shu, L. Zhao, X. Shi, W. Liu, D. Shi, and F. Kong, "Torsional wave propagation in a circular plate of piezoelectric radial phononic crystals," J. Appl. Phys. **118**(18), 184904 (2015).
[8] A. A. Maznev, "Band gaps and Brekhovskikh attenuation of laser-generated surface acoustic waves in a patterned thin film structure on silicon," Phys. Rev. B **78**, 155323 (2008).
[9] I. A. Veres and T. Berer, "Complexity of band structures: Semi-analytical finite element analysis of one-dimensional surface phononic crystals," Phys. Rev. B **86**, 104304 (2012).
[10] S. Sadat-Saleh, S. Benchabane, F. Issam Baida, M.-P. Bernal, and V. Laude, "Tailoring simultaneous photonic and phononic band gaps," J. Appl. Phys. **106**, 074912 (2009).
[11] N. Papanikolaou, I. E. Psarobas, and N. Stefanou, "Absolute spectral gaps for infrared light and hypersound in three-dimensional metallodielectric phoxonic crystals," Appl. Phys. Lett. **96**, 231917 (2010).
[12] J. N. Gillet, Y. Chalopin, and S. Volz, "Atomic-scale three-dimensional phononic crystals with a very low thermal conductivity to design crystalline thermoelectric devices," J. Heat Transfer **131**, 043206 (2009).
[13] P. E. Hopkins, C. M. Reinke, M. F. Su, R. H. Olsson III, E. A. Shaner, Z. C. Leseman, J. R. Serrano, L. M. Phinney, and I. El-Kady, "Reduction in the thermal conductivity of single crystalline silicon by phononic crystal patterning," Nano Lett. **11**, 107 (2011).
[14] T. Zhu and E. Ertekin, "Phonon transport on two-dimensional graphene/boron nitride superlattices," Phys. Rev. B **90**(19), 195209 (2014).
[15] T. Zhu and E. Ertekin, "Resolving anomalous strain effects on two-dimensional phonon flows: The cases of graphene, boron nitride, and planar superlattices," Phys. Rev. B **91**, 205429 (2015).
[16] M. Maldovan, "Sound and heat revolutions in phononics," Nature **503**, 209 (2013).
[17] Z. Liu, X. Zhang, Y. Mao, Y. Y. Zhu, Z. Yang, C. T. Chan, and P. Sheng, "Locally resonant sonic crystal," Science **289**, 1734 (2000).
[18] Y. Wu, Y. Lai, and Z.-Q. Zhang, "Effective medium theory for elastic metamaterials in two dimensions," Phys. Rev. B **76**, 205313 (2007).
[19] R. Zhu, X. N. Liu, G. L. Huang, H. H. Huang, and C. T. Sun, "Microstructural design and experimental validation of elastic metamaterial plates with anisotropic mass density," Phys. Rev. B **86**, 144307 (2012).
[20] E. D. Nobrega, F. Gautier, A. Pelat, and J. M. C. Dos Santos, "Vibration band gaps for elastic metamaterial rods using wave finite element method," Mech. Syst. Signal Process. **79**, 192 (2016).
[21] M. Farhat, S. Guenneau, and S. Enoch, "Ultrabroadband elastic cloaking in thin plates," Phys. Rev. Lett. **103**, 024301 (2009).
[22] N. Stenger, M. Wilhelm, and M. Wegener, "Experiments on elastic cloaking in thin plates," Phys. Rev. Lett. **108**, 014301 (2012).
[23] R. Zhu, X. N. Liu, G. K. Hu, C. T. Sun, and G. L. Huang, "Negative refraction of elastic waves at the deep-subwavelength scale in a single-phase metamaterial," Nat. Commun. **5**, 5510 (2014).
[24] M. Dubois, M. Farhat, E. Bossy, S. Enoch, S. Guenneau, and P. Sebbah, "Flat lens for pulse focusing of elastic waves in thin plates," Appl. Phys. Lett. **103**, 071915 (2013).
[25] M. Dubois, E. Bossy, S. Enoch, S. Guenneau, G. Lerosey, and P. Sebbah, "Time-driven superoscillations with negative refraction," Phys. Rev. Lett. **114**, 013902 (2015).
[26] G. Ma and P. Sheng, "Acoustic metamaterials: From local resonances to broad horizons," Sci. Adv. **2**, e1501595 (2016).
[27] X. Wang, "Dynamic behavior of a metamaterial system with negative mass and modulus," Int. J. Solids Struct. **51**, 1534 (2014).
[28] J. H. Oh, Y. E. Kwon, H. J. Lee, and Y. Y. Kim, "Elastic metamaterials for independant realization of negativity in density and stiffness," Scientific Reports **6**, 23630 (2016).
[29] C.-N. Weng, P.-W. Chang, and T. Chen, "Numerical simulation of broadband bi-negative elastic metamaterials and wave transmission properties," Proc. Eng. **79**, 622 (2014).
[30] H. H. Huang, C. T. Sun, and G. L. Huang, "On the negative effective mass density in acoustic metamaterials," Int. J. Eng. Sci. **47**, 610 (2009).
[31] Y. Wu, Y. Lai, and Z.-Q. Zhang, "Elastic metamaterials with simultaneously negative effective shear modulus and mass density," Phys. Rev. Lett. **107**, 105506 (2011).
[32] Y. Ding, Z. Liu, C. Qiu, and J. Shi, "Metamaterial with simultaneously negative bulk modulus and mass density," Phys. Rev. Lett. **99**, 093904 (2007).
[33] R. Zhu, X. N. Liu, and G. L. Huang, "Study of anomalous wave propagation and reflection in semi-infinite elastic metamaterials," Wave Motion **55**, 73 (2015).
[34] S. J. Mitchell, A. Pandolfi, and M. Ortiz, "Metaconcrete: Designed aggregates to enhance dynamic performance," J. Mech. Phys. Solids **65**, 69 (2014).
[35] N. Aravantinos-Iafiris and M. M. Sigalas, "Large scale phononic metamaterials for seismic isolation," J. Appl. Phys. **118**, 064901 (2015).
[36] K. T. Tan, H. H. Huang, and C. T. Sun, "Blast-wave impact mitigation using negative effective mass density concept of elastic metamaterials," Int. J. Impact Eng. **64**, 20 (2014).
[37] S.-H. Kim and M. P. Das, "Artificial seismic shadow zone by acoustic metamaterials," Mod. Phys. Lett. B **27**(20), 1350140 (2013).
[38] O. R. Bilal and M. I. Hussein, "Trampoline metamaterial: Local resonance enhancement by springboards," Appl. Phys. Lett. **103**, 111901 (2013).
[39] J. Y. Yoritomo, R. L. Weaver, P. Roux, M. Rupin, and E. G. Willams, "On band gap predictions for multiresonant metamaterials on plates," J. Acoust. Soc. Am. **139**(3), 1282–1284 (2016).
[40] A. Colombi, P. Roux, and M. Rupin, "Sub-wavelength energy trapping of elastic waves in a metamaterial," J. Acoust. Soc. Am. **136**(2), EL192–EL198 (2014).
[41] R. Zhu, X. N. Liu, G. K. Hu, F. G. Yuan, and G. L. Huang, "Microstructural designs of plate-type elastic metamaterial and their potential applications: A review," Int. J. Smart Nano Mater. **6**(1), 14–40 (2015).
[42] X. N. Liu, G. K. Hu, G. L. Huang, and C. T. Sun, "An elastic metamaterial with simultaneously negative mass density and bulk modulus," Appl. Phys. Lett. **98**, 251907 (2011).
[43] J. Achenbach, *Wave Propagation in Elastic Solids* (North-Holland Publications Co. 1973), Vol. 16(2), p. 544.